Supplement of

Characterization of aerosol hygroscopicity, mixing state, and CCN activity at a suburban site in the central North China Plain

Yuying Wang[1], Zhanqing Li[1], Yingjie Zhang[2], Wei Du[2,3], Fang Zhang[1] , Haobo Tan[4], Hanbing Xu[5], Xiaoai Jin[1], Xinxin Fan[1], Zipeng Dong[1], Qiuyan Wang[6], Yele Sun[2,3]

[1]College of Global Change and Earth System Science, Beijing Normal University, Beijing 100875, China

[2]State Key Laboratory of Atmospheric Boundary Layer Physics and Atmospheric Chemistry, Institute of Atmospheric Physics, Chinese Academy of Sciences, Beijing 100029, China

[3]College of Earth Sciences, University of Chinese Academy of Sciences, Beijing 100049, China

[4]Key Laboratory of Regional Numerical Weather Prediction, Institute of Tropical and Marine Meteorology, China Meteorological Administration, Guangzhou 510080, China

[5]Shared Experimental Education Center, Sun Yat-sen University, Guangzhou 510275, China

[6]Collaborative Innovation Center on Forecast and Evaluation of Meteorological Disasters, Nanjing University of Information Science and Technology, Nanjing, 210044, China

**Correspondence to*: Zhanqing Li (zli@atmos.umd.edu)

Table S1. Gravimetric densities (ρ) and hygroscopicity parameters (κ) used in this study.

Species	NH_4NO_3	$(NH_4)_2SO_4$	NH_4HSO_4	H_2SO_4	POA	SOA	BC
ρ (kg m^{-3})	1720	1769	1780	1830	1000	1400	1700
κ	0.67	0.61	0.61	0.9	0	0.1	0

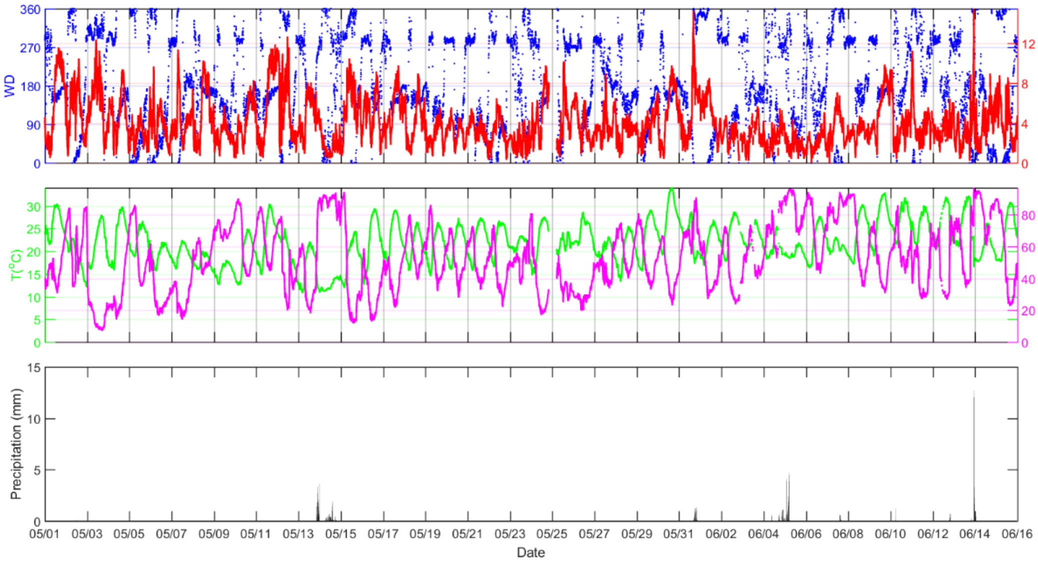

Figure S1. Time series of different meteorological variables measured at the site: wind direction (WD), wind speed (WS), ambient temperature (T), relative humidity (RH), and the amount of precipitation.

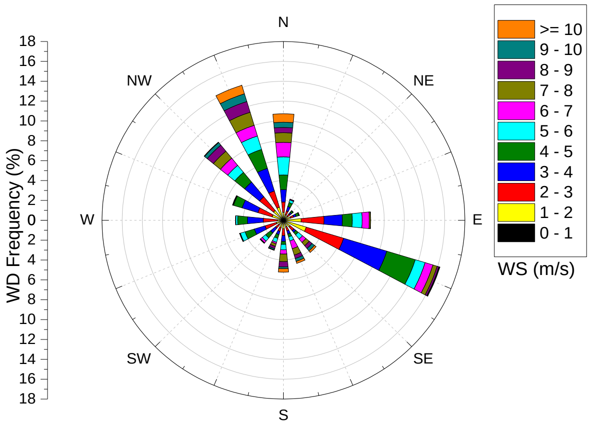

Figure S2. Wind rose diagram summarizing wind directions (WD) and wind speeds (WS) during the measurement period.

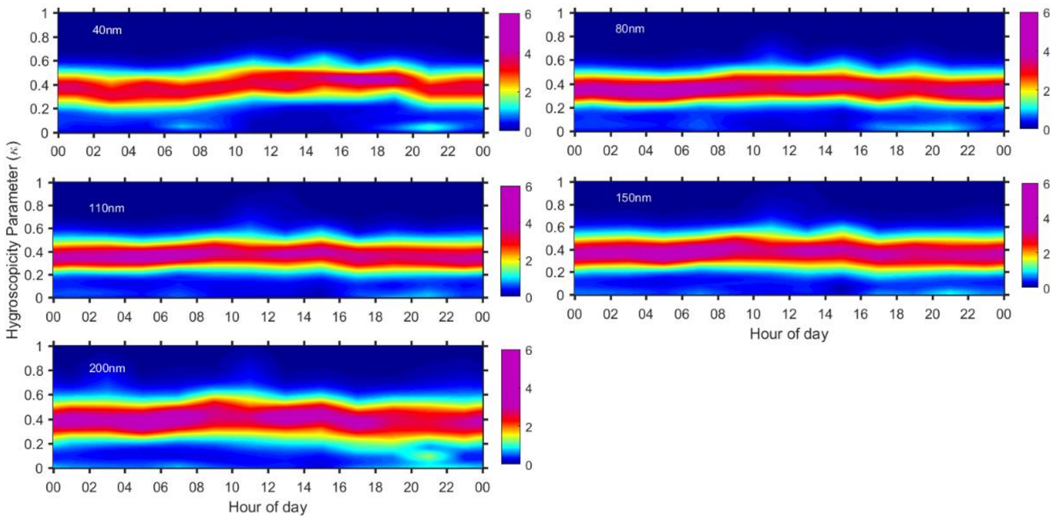

Figure S3. Diurnal variations in the probability density functions of κ_{gf} (κ-PDF) for different particle sizes.

Figure S3 shows the diurnal variations in κ-PDF for different particle sizes. Unimodal distributions are seen. Two or three modes occasionally appear at night. This is likely because photochemical reactions are weak then and the newly effluent hydrophobic species (such BC and organics) cannot quickly mix with inorganic salts.

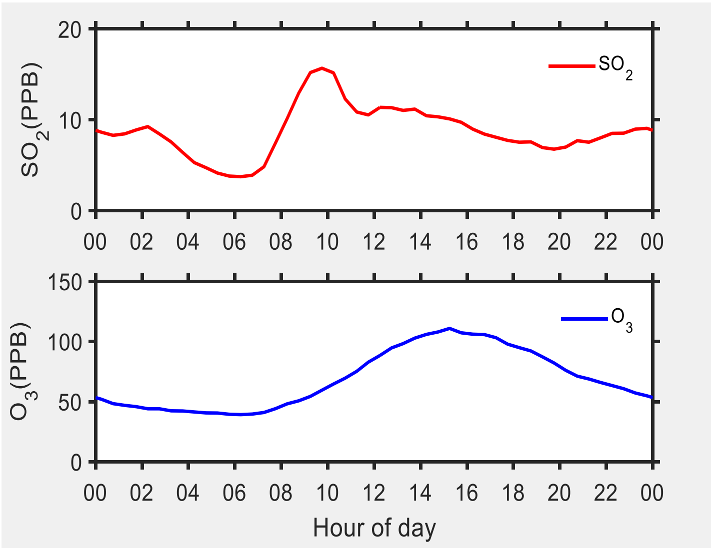

Figure S4. Diurnal variations in mean SO_2 and O_3 concentrations.

Figure S4 shows the diurnal variations in mean SO_2 and O_3 concentrations. Affected by the mountain-valley wind, prevailing winds shift from the northwest to the southeast in the early morning. There are more industrial emissions to the southeast of the measurement site than to the northwest of the site. Therefore, the SO_2 concentration increases sharply in the morning after the wind shift. The O_3 concentration increases gradually after sunrise when photochemical reactions begin to occur and strengthen during the day. This likely explains the frequent occurrence of NPF events and the increase in sulfate during the day at XT.

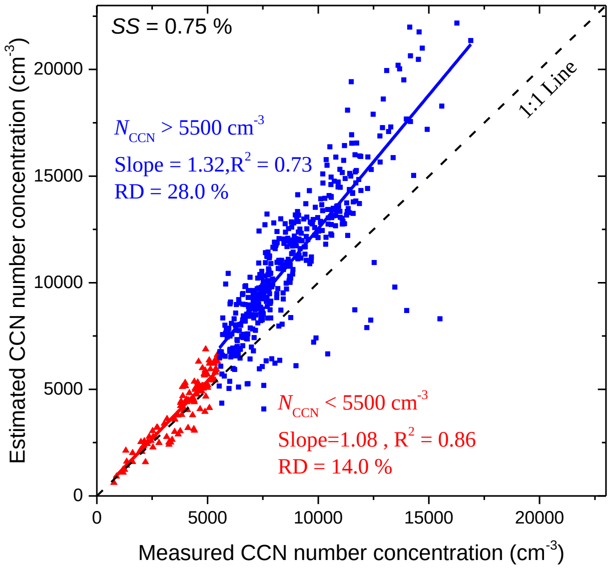

Figure S5. Estimated versus measured CCN number concentrations at SS = 0.75 % (Fig. 9-a4). The N_{CCN} is estimated based on κ-Köhler theory, using the real-time κ_{chem}. Here, the critical value of N_{CCN} = 5500 cm^{-3} is used to separate the points into two groups. A separate linear regression analysis is done on each group. The slopes, correlation coefficients (R^2), and relative deviations (RD) are shown in the figure.

Figure S5 shows that the linear regression is better when N_{CCN} < 5500 cm^{-3}. The slope and RD for N_{CCN} < 5500 cm^{-3} are much lower than the values calculated using all N_{CCN} data (section 4.4 in the paper), while the values for N_{CCN} > 5500 cm^{-3} are higher. This suggests that the CCN deviations are mainly caused by the overestimation of N_{CCN} due to measurement uncertainties (section 4.4).

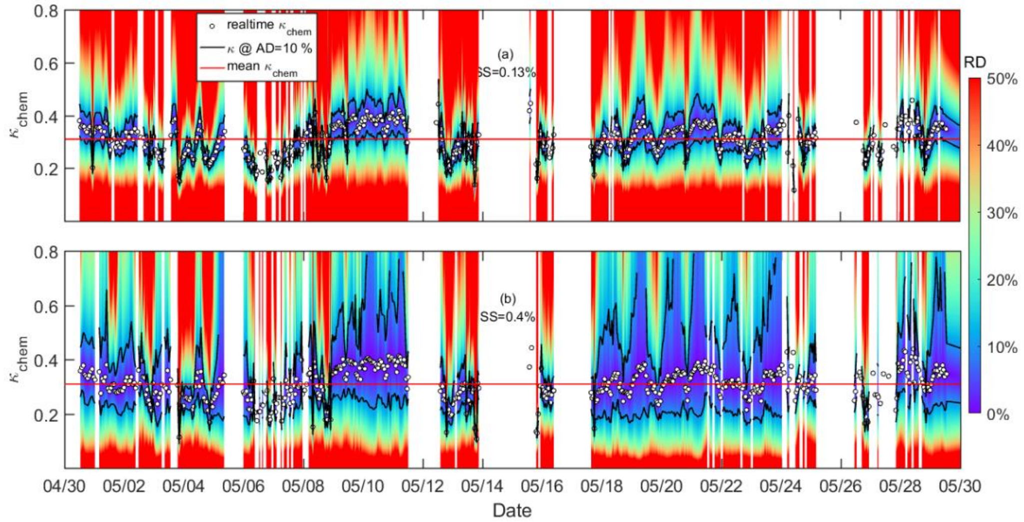

Figure S6. Sensitivity of N_{CCN} estimates to κ_{chem} as a function of time at (a) SS = 0.13 % and (b) SS = 0.40 %. More information about the plot can be found in the Fig. 10 caption.